Journal of Applied Mechanics and Technical Physics, Vol. 49, No. 3, pp. 425–436, 2008

MOTION AND HEAT AND MASS TRANSFER IN A DISPERSE ADMIXTURE IN TURBULENT NONISOTHERMAL JETS OF A GAS AND A LOW-TEMPERATURE PLASMA

K. N. Volkov

UDC 532.529:536.24

The motion and heat and mass transfer of particles of a disperse admixture in nonisothermal jets of a gas and a low-temperature plasma are simulated with allowance for the migration mechanism of particle motion actuated by the turbophoresis force and the influence of turbulent fluctuations of the jet flow velocity on heat and mass transfer of the particle. The temperature distribution inside the particle at each time step is found by solving the equation of unsteady heat conduction. The laws of scattering of the admixture and the laws of melting and evaporation of an individual particle are studied, depending on the injection velocity and on the method of particle insertion into the jet flow. The calculated results are compared with data obtained with ignored influence of turbulent fluctuations on the motion and heat and mass transfer of the disperse phase.

Key words: *turbulence, particle, jet, heat and mass transfer, numerical simulation.*

Introduction. Plasma spraying, being an effective method for recovering and hardening of surfaces of elements of various machines and mechanisms, allows coatings to be formed from various materials and ensures a wide range of physical, chemical, and application properties.

The motion and heating of particles in the jet, which exert a significant effect on coating formation, have to be studied in detail. The influence of the target on the jet flow is substantial at a distance of several jet diameters from the surface, which involves only minor changes in particle diameters because of their inertia.

Rarefied gas–particle flows with no allowance for interaction of particles and their effect on the gas flow are often modeled by the discrete trajectory method of test particles [1]. Depending on the method used to take into account the effect of carrier flow turbulence on particle motion, the deterministic and stochastic versions of the discrete trajectory approach are distinguished [2].

In the deterministic approach, the particle location at the initial time completely determines its further evolution. Particle interaction with turbulent moles is ignored, which is valid only for sufficiently inertial particles. For flows with curved streamlines, which involve melting and combustion of particles, the model yields high errors in determining the characteristics of the two-phase flow [1, 2].

In the stochastic approach, the influence of turbulent fluctuations is taken into account by adding random fluctuations of the carrier flow velocity to the equation of motion of the test particle [2–4]. Particle interaction with turbulent moles leads to randomization of particle motion, and the particle location at a given time is determined only by the probability of its residence in one of the possible states at each next time. A large number of test particles have to be calculated to obtain a statistically reliable averaged pattern of particle motion.

Application of the stochastic variant of the discrete trajectory approach for calculating nonisothermal jet systems [3, 4] offers an explanation for some experimentally observed anomalous phenomena [5, 6], such as formation of particle "filaments" in the axial region of the jet and entrainment of particles outside the jet in the case of their streamwise injection at the nozzle exit.

University of Surrey, Guildford, UK; k.volkov@surrey.ac.uk; dsci@mail.ru. Translated from Prikladnaya Mekhanika i Tekhnicheskaya Fizika, Vol. 49, No. 3, pp. 95–108, May–June, 2008. Original article submitted November 9, 2006; revision submitted April 17, 2007.

Models of different degrees of complexity have been developed for calculating gas–particle jets within the framework of the discrete trajectory approach [7–10]. In many applications, particle heating, melting, and evaporation are simulated by a simplified approach, which implies that the thermal conductivity of the particle material is infinitely large, and the temperature gradient inside the particle is neglected [2, 3, 8, 9, 11] (thermally "thin" particle). The particle temperature is averaged over its volume and changes only in time; the loss of the particle mass due to evaporation and its influence on particle motion are ignored. The assumption on the nonisothermal character of coarse particles ($r_p \approx 50$ μm) is a simplifying assumption, but it is not properly justified [12].

Other approaches involve solutions obtained from the condition of the heat balance on the particle surface [12] or models with semi-empirical relations used to calculate the radius of the evaporating particle [11]. For the calculation accuracy to be improved, an equation of unsteady heat conduction inside the particle with appropriate initial and boundary conditions is solved [13] (thermally "thick" particle). Parabolic approximation of the temperature field is often used to simplify the solution of the problem with allowance for a finite thermal conductivity of the particle material [14] (the parabolic temperature profile does not satisfy the heat-conduction equation, but satisfies the condition of the heat balance on the droplet surface). If the heat-transfer coefficient is constant, the exact solution is obtained; for an arbitrary value of the heat-transfer coefficient, an integral equation has to be solved [15].

The migration mechanism of particle motion and the influence of turbulent fluctuations of velocity of the carrier jet flow on particle heating, melting, and evaporation are usually ignored.

The present paper describes the influence of various factors on acceleration, heating, melting, and evaporation of particles in a nonisothermal jet flow. The effect of turbulence on the behavior of the disperse admixture is taken into account by introducing random fluctuations of velocity of the jet flow to equations that describe the motion and heat and mass transfer of an individual particle. The temperature distribution inside the particle is found from the equation of unsteady heat conduction, which is solved at each time step. The influence of conditions of flow exhaustion from the nozzle and insertion of particles into the jet flow on the laws of scattering, heating, melting, and evaporation of an individual particle is studied. Numerical results are compared with data obtained with no allowance made for the effect of turbulent fluctuations on the motion and heat and mass transfer of the disperse phase.

Simulation of the Carrier Phase. Let us consider scattering and heat and mass transfer of spherical particles in jets of a gas and a low-temperature plasma. The influence of the disperse phase on the carrier flow is ignored. The plasma is presented as an ideal compressible gas and is assumed to be optically thin.

Let us align the x axis of a cylindrical coordinate system with the axis of symmetry of the jet. The origin is placed at the nozzle exit. The variables with the length dimension are normalized to the nozzle-exit radius r_a, and the scales for the variables with the velocity and temperature dimensions are the gas velocity U_a and the temperature T_a at the nozzle exit.

The model for calculating the parameters of the carrier jet flow is chosen on the basis of the overheat parameter $\vartheta_a = h_a/h_\infty$.

The statistical characteristics of turbulence for moderately heated jets ($\vartheta_a < 2$–3) are calculated by the Reynolds-averaged Navier–Stokes equations written in the approximation of a nonisothermal boundary layer and the k–ε turbulence model [3, 4] (the correction to the constant in the formula for turbulent viscosity is taken into account). The radial velocity and temperature profiles at the nozzle exit are defined at the form

$$U_a(r) = U_a[1 - (r/r_a)^{n_1}], \qquad T_a(r) = T_a[1 - (r/r_a)^{n_2}],$$

where $n_1 = 1.2$ and $n_2 = 6$ [7]. For the turbulent kinetic energy and its dissipation rate, the radial distributions at the nozzle exit are taken in the form

$$k_a(r) = [U_a(r)\theta_a]^2/2, \qquad \varepsilon_a(r) = c_\mu k_a(r)^{3/2}/L_a,$$

where θ_a and $L_a = 0.075 r_a$ are the degree and scale of turbulence at the nozzle exit [9].

For low-temperature plasma jets ($\vartheta_a = 3$–12), the mean flow of the carrier medium is simulated by the method of integral relations [4, 16]. The statistical characteristics of turbulence are determined by an approximate approach based on processing the data on the microstructure of jet flows [3, 4]. The main semi-empirical relations that describe the distributions of the statistical characteristics of turbulence in submerged jets are given in [4, 16]. The nonisotropic character of turbulent fluctuations of the jet flow is taken into account by the approach developed

in [4] (the crossflow and circumferential components of velocity fluctuations amount to 70% of the streamwise component). The empirical dependence obtained in [2] is used to calculate the scale of turbulence.

The upper limit of the parameter ϑ_a separating the regions where the solution is constructed by different methods (k–ε turbulence model and method of integral relations) is rather conventional and depends on the method of discretization of the governing equations used to ensure stability of numerical simulations.

Particle Motion. The equations that describe the motion of a spherical test particle have the form

$$\frac{d\boldsymbol{r}_p}{dt} = \boldsymbol{v}_p; \tag{1}$$

$$\frac{d\boldsymbol{v}_p}{dt} = \frac{3C_D\rho}{8\rho_p r_p}\,|\boldsymbol{v}-\boldsymbol{v}_p|(\boldsymbol{v}-\boldsymbol{v}_p) - \frac{\boldsymbol{v}_p}{m_p}\,\frac{dm_p}{dt}. \tag{2}$$

For $\mathrm{Re}_p \leqslant 10^3$, the drag coefficient is determined by the formula [17]

$$C_D = 24(1 + 0.179\,\mathrm{Re}_p^{0.5} + 0.013\,\mathrm{Re}_p)f/\,\mathrm{Re}_p\,.$$

The function f takes into account the influence of the temperature dependence of thermophysical properties of the medium on the particle drag:

$$f = [\rho_\infty\mu_\infty/(\rho_w\mu_w)]^{0.6}.$$

For the relative motion of the gas and particle, the Reynolds number is found by the formula

$$\mathrm{Re}_p = 2r_p\rho|\boldsymbol{v}-\boldsymbol{v}_p|/\mu.$$

The effect of turbulence of the carrier flow on the behavior of the disperse phase is taken into account by inserting random fluctuations of the carrier flow velocity into Eq. (2). For this purpose, the model of particle interaction with turbulent moles is used [2].

The turbulence field is simulated by a set of spherical vortices. Each vortex is characterized by a certain velocity, size, and time of existence:

$$\boldsymbol{v}_e = \{u_e, v_e, w_e\}, \qquad L_e = 0.16k^{3/2}/\varepsilon, \qquad t_e = L_e/(2k/3)^{1/2}.$$

The moving gas mole entrains the trapped particles. The mole retains the fluctuating velocity during the time of its existence (from the moment the mole leaves one layer of the flow until it becomes mixed with another layer), losing and acquiring its properties in a jumplike manner.

The vortex velocity is decomposed into the mean and fluctuating components. The mean velocity is calculated by integrating the Reynolds-averaged Navier–Stokes equations. The fluctuating velocity is chosen from the normal distribution of the probability with a zero mathematical expectation and a variance corresponding to the turbulent kinetic energy. The resultant value is multiplied by a damping function, which takes into account the nonisotropic character of turbulence and which is constructed on the basis of data on the microstructure of jet flows [3, 4, 16].

Let a particle moving with a velocity $\boldsymbol{v}_p$ at the time t_i be located at the center of the vortex moving with a velocity $\boldsymbol{v}_e$ (Fig. 1). With allowance for the relative motion of the vortex and particle, three situations are possible at the time t_{i+1}: 1) the particle stays within the initial turbulent mole and moves together with the latter ($r < L_e$); 2) the particle leaves the limits of the initial turbulent mole ($r > L_e$); 3) the time of existence of the vortex is exhausted, and the mole properties change ($t_{i+1} - t_i > t_e$); the particle is trapped by a new turbulent mole, and a new interaction begins. In case 1, new values of the characteristic scales of the vortex (velocity, size, and time of existence) are calculated in accordance with the new particle location and new local characteristics of turbulence. In case 2 and case 3, the particle is trapped by a new turbulent mole with different characteristics. A new fluctuation of the carrier flow velocity is sampled.

The time needed for the particle to go outside the initial mole is estimated by the linearized equation of motion of the particle [1, 2]

$$t_c = -\tau_p \ln\,[1 - L_e/(t_p|\boldsymbol{v}-\boldsymbol{v}_p|)].$$

The time of dynamic relaxation of the particle is calculated by the relation

$$t_p = 8\rho_p r_p/(3\rho C_D|\boldsymbol{v}-\boldsymbol{v}_p|).$$

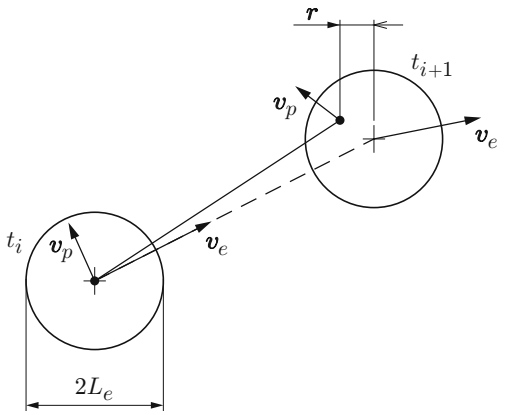

Fig. 1. Particle–turbulent mole interaction for the particle remaining within the initial fluctuating mole ($r < L_e$ and $t_{i+1} - t_i < t_e$).

If $L_e > t_p|\boldsymbol{v} - \boldsymbol{v}_p|$, then the expression for t_c becomes meaningless. This means that the particle stays inside a given vortex as long as the latter exists. The time criterion of generation of a new fluctuation is the time of vortex existence t_e or the time of particle transition through the vortex t_c, whichever is smaller:

$$t = \begin{cases} \min(t_e, t_c), & L_e > t_p|\boldsymbol{v} - \boldsymbol{v}_p|, \\ t_e, & L_e \leqslant t_p|\boldsymbol{v} - \boldsymbol{v}_p|. \end{cases}$$

The integral scale of turbulence is used as a spatial criterion.

Equations (1) and (2) are integrated along the trajectory of an individual particle and require only the initial conditions to be set (the particle coordinates and velocity at the time $t = 0$). The carrier gas velocity is a random function of spatial coordinates and time. The model is supplemented by equations that describe particle heating, melting, and evaporation.

Particle Heating, Melting, and Evaporation. Depending on the carrier flow parameters and the particle size, the models of thermally "thin" or thermally "thick" particles are used.

The areas of applicability of the approximations of the thermally "thin" and thermally "thick" particles are established by comparing the characteristic time of reconstruction (equalization) of the temperature field inside the particle $t_p = c_p^m \rho_p r_p^2/\lambda_p$ with the characteristic time of changes in the thermal conditions near the particle $t = \min\{t_\vartheta, t_t\}$ (t_ϑ is the time of thermal relaxation and t_t is the characteristic time scale of turbulent vortices). The estimates yield $t_t \ll t_\vartheta$. If we assume that $t_t \approx 10^{-5}$ sec, then we obtain $t/t_p = 10^3$–10^{-1} for metal particles (for aluminum particles, $t_p = 10^{-8}$ for $r_p = 1$ μm and $t_p = 10^{-4}$ for $r_p = 100$ μm). The transition from one model to the other occurs in calculations at $t/t_p = 0.8$.

Thermally "Thin" Particle. The equation of temperature changes, which describes convective and radiant heat transfer between the spherical particle and the carrier gas, is written as

$$\frac{dT_p}{dt} = \frac{3}{c_p^m \rho_p r_p}\left[\alpha(T - T_p) - \psi\sigma(T_p^4 - T^4)\right] - \frac{\Lambda_m}{c_p^m m_p}\frac{dm_p}{dt}, \tag{3}$$

where c_p^m is the specific heat of the particle material, ψ is the emissivity of the particle surface, and Λ_m is the specific heat of melting. The heat-transfer coefficient of the particle α is expressed via the Nusselt number $\mathrm{Nu}_p = 2r_p\alpha/\lambda$ calculated by the dependence [17]

$$\mathrm{Nu}_p = (2 + 0.459\,\mathrm{Re}_p^{0.55}\,\mathrm{Pr}^{\,0.33}) f g_1 g_2.$$

The function g_1 takes into account that the thermophysical properties of the medium are temperature-dependent; the function g_2 takes into account the correction on particle evaporation:

$$g_1 = \frac{c_{p\infty}}{c_{pw}}, \qquad g_2 = \frac{\Lambda_v}{h_\infty - h_w}\ln\left(1 + \frac{h_\infty - h_w}{\Lambda_v}\right)$$

(Λ_v is the latent heat of evaporation).

Let us denote the relative melted mass of the particle by $z_p = 1 - m_p/m_{p0}$. When the melting point T_m is reached, the particle temperature ceases to change ($dT_p/dt = 0$), and the particle melting is described by the equation

$$\frac{dz_p}{dt} = \frac{3}{\rho_p r_p \Lambda_m} [\alpha(T - T_m) - \psi\sigma(T_p^4 - T^4)]. \tag{4}$$

The particle temperature is calculated by Eq. (3) for $T_p < T_m$ and $T_m < T_p < T_v$ and by Eq. (4) for $T_p = T_m$.

The amount of heat necessary for complete melting of the particle (at $T_p \geqslant T_m$) is

$$Q_m = m_p \int\limits_{T_0}^{T_m} c_p^m \, dT + m_p \Lambda_m.$$

The criteria of complete melting and evaporation of the particle have the form

$$\int\limits_0^t Q dt \geqslant Q_m, \qquad \int\limits_0^t Q dt \geqslant Q_m + m_p \int\limits_{T_m}^{T_v} c_p^m \, dT + m_p \Lambda_v.$$

Thermally "Thick" Particle. At $0 \leqslant r \leqslant r_w$ and $t > 0$, the temperature field inside the particle is described by the unsteady heat conduction equation in spherical coordinates:

$$\rho_p c_p^m \frac{\partial T_p}{\partial t} = \frac{1}{r^2} \frac{\partial}{\partial r}\Big(r^2 \lambda_p \frac{\partial T_p}{\partial r}\Big) + S(r).$$

The source term $S(r)$, which takes into account the absorption of radiation by the droplet, is calculated in the general case on the basis of the Mie theory. Various approximate relations are used to simplify the calculations [15]. The presence of an additional heat source described by the term $S(r)$ increases the rate of evaporation. In the present model, the source term is ignored.

A uniform temperature distribution $T_p(r, 0) = T_{p0}$ is set at the initial time. The boundary conditions at the particle center follow from the condition of symmetry

$$\frac{\partial T}{\partial r}\Big|_{r=0} = 0.$$

The melting surface is subjected to the condition

$$\Big(\lambda_p \frac{\partial T}{\partial r}\Big)\Big|_{r=r_w^-} - \Big(\lambda_p \frac{\partial T}{\partial r}\Big)\Big|_{r=r_w^+} = \rho_p \Lambda_m \frac{dr_w}{dt}.$$

The motion of the melting front is described by the equation

$$\frac{dr_w}{dt} = \chi(T_m - T_w),$$

where T_w is the surface temperature and χ is the kinetic coefficient, which takes into account the nonequilibrium character of the process [in real processes, $\chi = 0.01$–0.85 m/(K · sec), depending on the particle material].

The boundary conditions on the particle surface take into account particle heating due to convective and radiant fluxes from the gas phase and cooling due to evaporation:

$$4\pi r_w^2 \Big(\lambda_p \frac{\partial T}{\partial r}\Big)\Big|_{r=r_w} = q_1 - q_2 - q_3.$$

Here $q_1 = 4\pi r_p^2 \alpha(T - T_w)$, $q_2 = \dot{m}_v \Lambda_v = -\rho_p \Lambda_v \dot{r}_p$, and $q_3 = 4\pi r_p^2 \psi\sigma(T_w^4 - T^4)$. The particle evaporation rate is determined by vapor diffusion through the boundary layer around the particle:

$$\dot{m}_v = 2\pi r_p \rho D \ln[(1 + B)\,\mathrm{Sh}]$$

(D is the diffusion coefficient and Sh is the Sherwood number). The mass-transfer parameter B depends on the mass fraction of vapor in the gas phase and vapor concentration on the particle surface.

Calculation Results. The volume concentration of particles in the calculations is smaller than 10^{-6}; therefore, the finite value of their volume concentration is ignored. The number of particles in the computational domain is unchanged.

The carrier flow parameters are calculated in the axisymmetric statement, whereas a three-dimensional problem is solved for particles. Simulations are performed for different numbers of trajectories of the test particles N_p (depending on the particle size) up to $N_p = 2.5 \cdot 10^4$. The error decreases by the law $N_p^{1/2}$. A comparison of results obtained with different numbers of realizations shows that a statistically independent pattern of particle motion is obtained at $N_p > 2 \cdot 10^4$ (a further increase in the number of particles changes the accuracy by less than 2.5%). The step of integration along each trajectory is bounded by the time and space scales of turbulence. A decrease in the particle size increases the number of realizations necessary to obtain a statistically reliable averaged pattern of particle motion because of the increased contribution of particle interactions with vortices of smaller sizes. The transition to the mean parameters is performed by averaging over a large number of particles.

To solve the Cauchy problem, we use methods that allow rapidly and slowly decaying components to be identified in the solution [18], which improves the efficiency of computations, as compared with the approaches proposed in [2–4]. To recover the gas parameters at points lying on the particle trajectory, we use the method of bilinear interpolation. The criterion of computation completion is the time when the particle leaves the computational domain (in the case of streamwise injection of particles), the time when the particle intersects the jet centerline (in the case of crossflow injection of particles), or the time of complete evaporation of the particle (in both cases).

Let us consider scattering and heating of aluminum oxide particles in a submerged jet of the air plasma with streamwise ($x = 0$ and $r/r_a = 0$, 0.5, and 1.0) and crossflow ($x = 0$ and $r/r_a = 1$) injection of particles at the nozzle exit. The following initial parameters of the gas and disperse phase are used: $r_a = 3$ mm, $U_a = 500$ m/sec, $T_a = 4700$ K, $U_{pa} = 0$–500 m/sec, $V_{pa} = 0$–10 m/sec, $T_{pa} = 300$ K, and $r_p = 5$–100 μm. The thermophysical properties of the gas and particles are taken from [19] (with allowance for their dependence on temperature).

The particle motion in a turbulent flow is determined by the turbulent Stokes number, which is the ratio of the time of dynamic relaxation of the particle to the characteristic time scale of turbulent vortices. In the case of motion of low-inertia particles of variable size, which obey the Stokes drag law, the Stokes number is no longer constant, and the analysis of the particle behavior becomes more complicated (the Stokes number is usually equal to the ratio of the particle relaxation time to the characteristic time of changes in the carrier flow parameters).

The results of computations characterizing scattering of particles in the region of jet expansion, depending on the particle size and place and velocity of particle injection at the nozzle exit are plotted in Figs. 2–4 (the solid curves are the results averaged over an ensemble of realizations). These results were obtained by the model of a thermally "thin" particle [3, 4] and illustrate the particle deviations from the mean trajectory.

In simulating the particle motion in the case of streamwise injection by the deterministic approach, the trajectories of heavy particles are lines parallel to the axis of symmetry of the jet (the crossflow component of jet flow velocity does not exert any significant effect on the motion of such particles).

The stochastic model takes into account the particle interaction with turbulent models. For fine particles ($r_p \approx 10$ μm), the inhomogeneity of the gas-phase turbulence field, which has a minimum of the kinetic energy, in the axial region of the jet leads to the onset of turbulent migration of the particle (turbophoresis force) in the direction of decreasing fluctuating energy of the gas, i.e., toward the jet axis. In the main part of the jet, the gradients of the turbulent kinetic energy near the jet axis are small, and the effect of turbophoresis becomes less pronounced.

For coarse particles ($r_p \approx 50$ μm), velocity fluctuations do not exert any significant effect on the particle motion in the entire region of jet expansion because of the high inertia of such particles. In this case, however, weak migration of particles toward the decreasing fluctuating energy of the gas is also observed.

A decrease in the initial velocity of particle motion (from U_a to zero) leads to more significant scattering of particles. Such a behavior is caused by the fact that particles with the initial velocity lower than the flow velocity move in the region with the maximum turbulent fluctuations (in the initial part of the jet) for a longer time. Shifting the coordinate of the point of particle injection to the nozzle exit shows that the most intense scattering of particles occurs if the particles are injected in the range of the coordinates $0 \leqslant r/r_a \leqslant 0.5$, while the least intense scattering is observed for $r/r_a = 1$.

With increasing distance from the nozzle exit, migration of particles toward the jet axis is supplemented by their scattering into the peripheral zone of the jet. In the far region of the jet with low-intensity migration, scattering of particles is mainly determined by processes of turbulent diffusion.

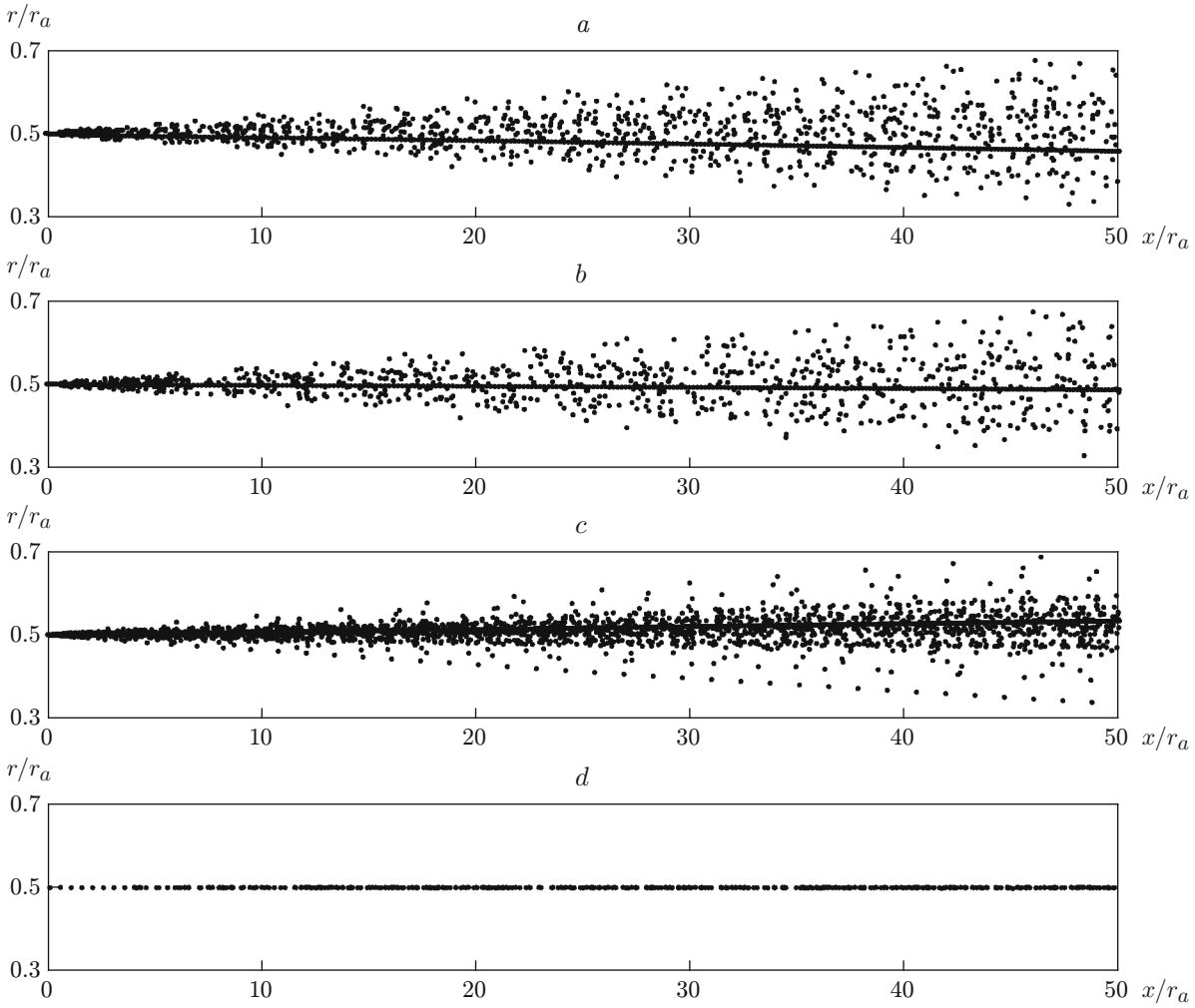

Fig. 2. Random trajectories of particles in the case of streamwise injection for $r = 0.5$ and $r_p = 10$ (a and b) and 50 μm (c and d); $U_{pa} = 0$ (a and c) and 500 m/sec (b and d).

The dynamic and thermal characteristics of the particle along the jet centerline, averaged over an ensemble of realizations, are plotted in Figs. 5 and 6 (the velocities and temperatures are normalized to the gas velocity U_a and temperature T_a at the nozzle exit). The points correspond to the results obtained by the deterministic model (with no allowance for the particle interaction with the fluctuating structure of the flow). In the initial cross section of the jet, we have $U_{pa} = U_a$, but the particle velocity decreases not as fast as the carrier flow velocity because of the particle inertia. In the main part of the jet, the particle temperature is higher than the carrier phase temperature. Owing to their high thermal inertia, it takes more time for the particles to cool down than for the gas.

For a given initial nonequilibrium distribution of velocities $U_a \neq U_{pa}$ (curves 1 and 2 in Fig. 5), an increase in the particle size from $r_p = 10$ μm to $r_p = 50$ μm deteriorates its melting (curve 2 in Fig. 5). A further increase in the particle temperature T_p after it reaches the plateau corresponding to the melting point of the aluminum oxide particle $T_m/T_a = 0.484$ means that the particle is completely melted.

Though the particle temperature is higher than the melting point, not all particles become melted.

An increase in the initial velocity of the injected particle also reduces particle heating. If the initial velocity of injection is high and the flow is equilibrium ($U_p = U_{pa}$), the particle temperature for the fractional composition used even does not reach the melting point (curve 3 in Fig. 5).

With allowance made for turbulent fluctuations, not all particles (having an identical initial size) injected at the nozzle exit become melted. Some particles either do not melt or have the melting radius with a nonmonotonic behavior in time (with simultaneous processes of melting and solidification).

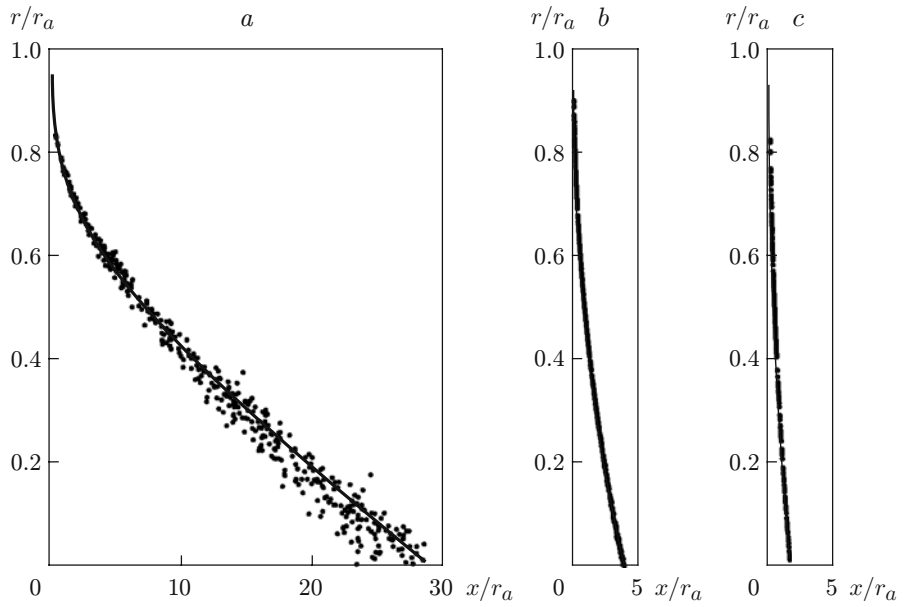

Fig. 3. Random trajectories of particles in the case of crossflow injection for $r_p = 30$ μm and $V_{pa} = 2$ (a), 4 (b), and 8 m/sec (c).

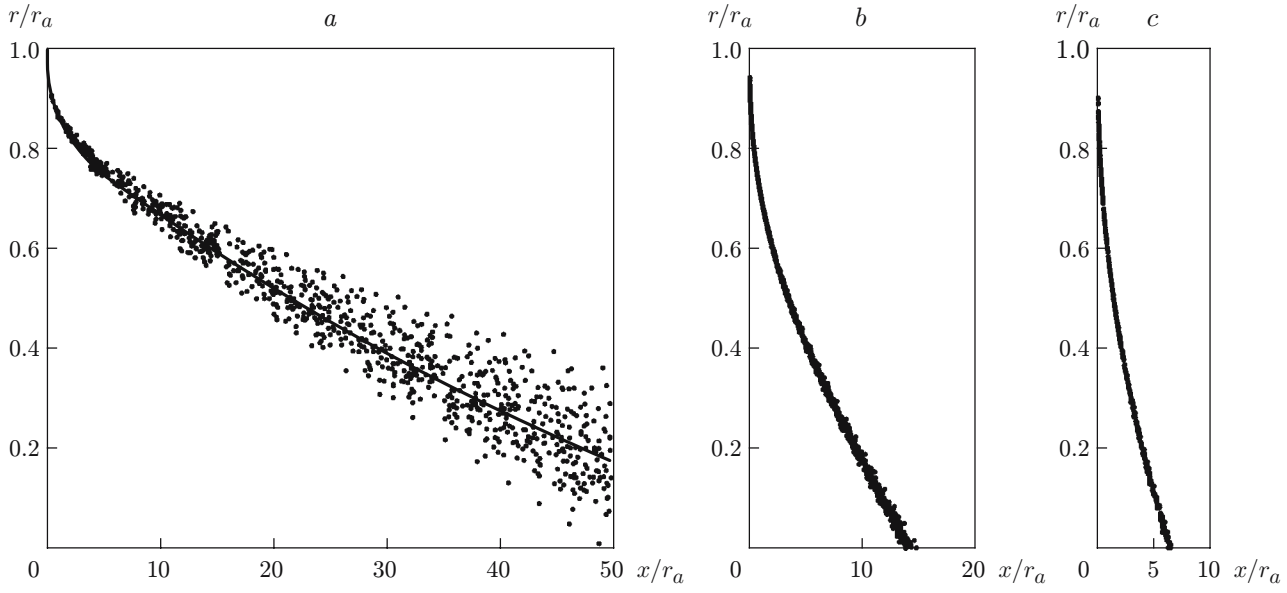

Fig. 4. Random trajectories of particles in the case of crossflow injection for $V_{pa} = 4$ m/sec and $r_p = 10$ (a), 30 (b), and 50 μm (c).

A typical feature of the dynamics of the particle moving along the jet centerline is its almost constant velocity for $x/r_a > 10$.

As the particle size decreases, their melting becomes more intense. In this case, however, the particles may be heated to a temperature much higher than the melting point. The maximum particle temperature is almost 110 K higher than the melting point. In the course of spraying, such overheating leads to undesirable splashing of droplets incident onto the surface.

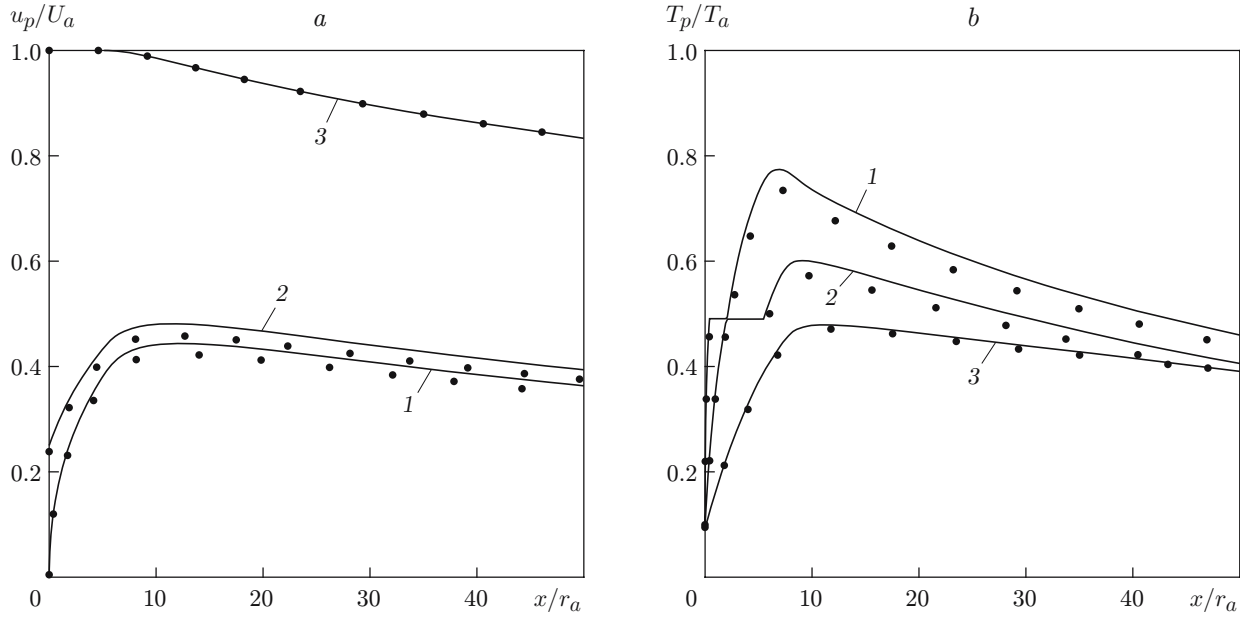

Fig. 5. Velocity (a) and temperature (b) of particles along the jet centerline in the case of streamwise injection for $r = 0$, $r_p = 10$ μm, and $U_{pa} = 0$ (1), 125 (2), and 500 m/sec (3); the points are the results calculated by the deterministic model.

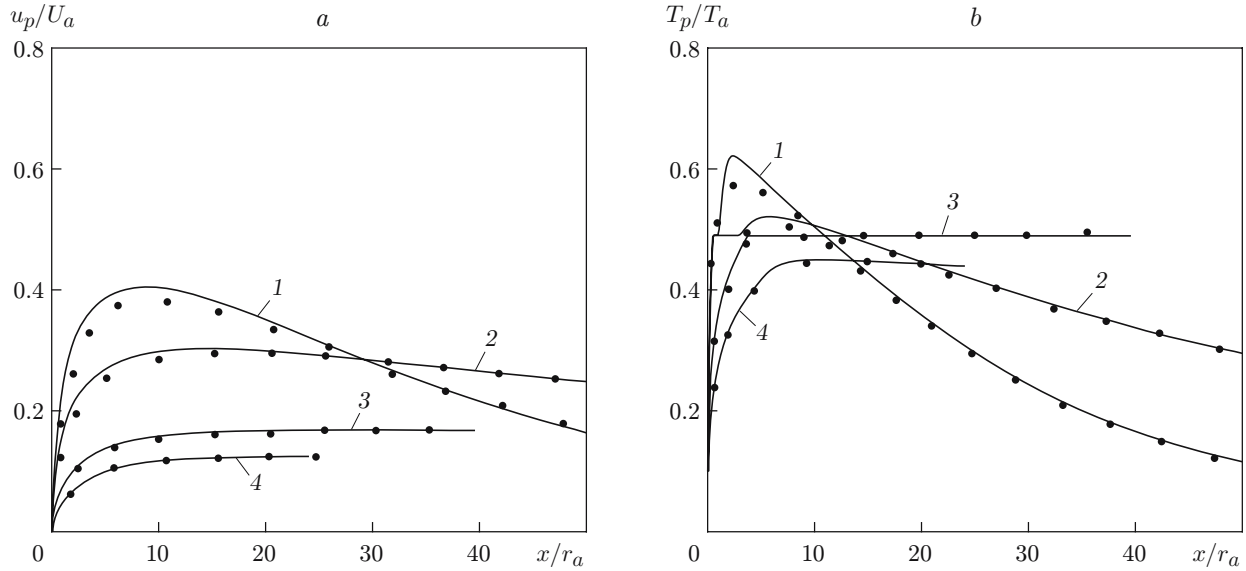

Fig. 6. Velocity (a) and temperature (b) of particles along the jet centerline in the case of crossflow injection for $r/r_a = 1$, $V_{pa} = 2$ m/sec, and $r_p = 5$ (1), 10 (2), 30 (3), and 50 μm (4); the points are the results calculated by the deterministic model.

The initial particle velocity has a weak effect on the time needed for the particle to reach the melting point t_m and evaporation point t_v (this also refers to the time of complete melting and evaporation of the particle). The dependences $t_m(r_p)$ and $t_v(r_p)$ are close in shape to parabolas.

At the same time, the initial velocity of particles has a significant effect on the axial coordinates of the points x_m and x_v corresponding to the beginning of particle melting and evaporation. The dependences of the coordinates x_m and x_v on the particle radius are close to parabolas, and the dependences of the velocities u_m and u_v acquired by the particles at these points on the particle radius are close to straight lines.

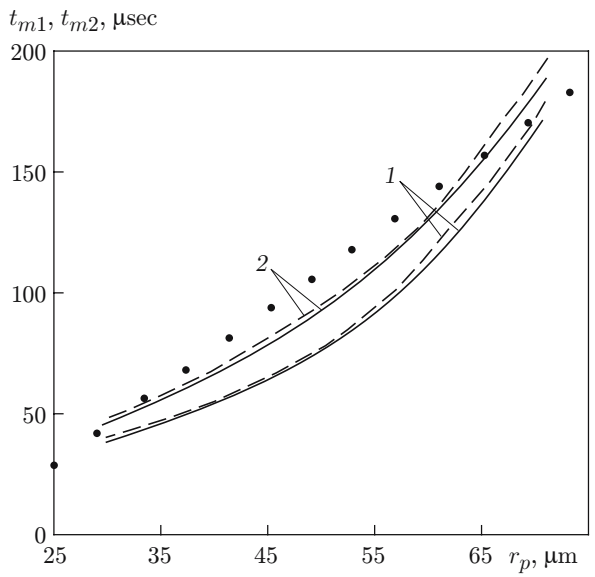

Fig. 7

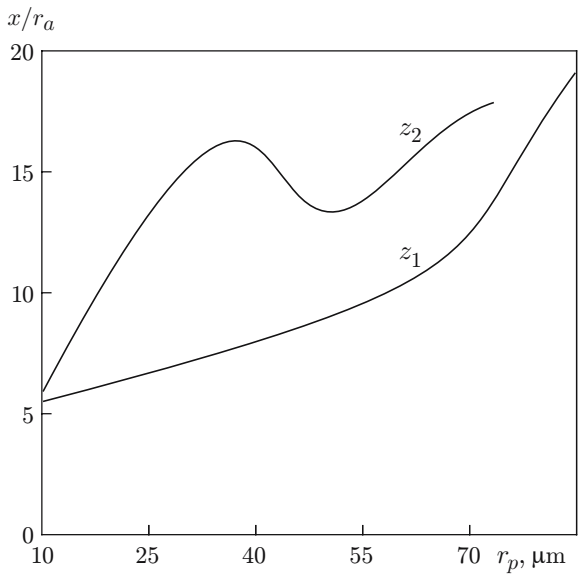

Fig. 8

Fig. 7. Parameters t_{m1} (1) and t_{m2} (2) characterizing particle melting versus the initial particle size: the solid and dashed curves show the results calculated by the stochastic and deterministic models, respectively; the points are the results calculated in [12].

Fig. 8. Parameters z_1 (1) and z_2 (2) characterizing particle evaporation versus the initial particle size.

An increase in the initial particle size increases the time needed for the particle to reach the melting and evaporation points. In the case of streamwise injection, the particles with $r_p > 20$ μm do not melt, and the particles with $r_p > 10$ μm do not reach the evaporation point for all values of U_{pa} (in the case of crossflow injection, the particles with $r_p > 30$ μm and $r_p > 10$ μm, respectively).

The particle melting begins at the time t_{m1} when the temperature of the particle surface reaches the melting point. This isothermal surface moves toward the particle center and reaches the latter at the time t_{m2} (the particle becomes melted at $t \approx 1.1 \cdot 10^{-4}$ sec). As the initial particle size increases, the values of the characteristic times increase (Fig. 7), and their dependences on the particle size are qualitatively identical; as the initial particle temperature increases, the characteristic times decrease. The results obtained agree with a similar dependence obtained in [12].

As the turbulent jet escaping from the nozzle becomes intensely mixed with the cold ambient medium and rapidly loses its heat content, the streamwise length of the zone of effective heating of the powder is 5–7 nozzle diameters. This length is insufficient for effective heating and melting of particles because of the small time of their residence in the high-temperature core of the jet.

Significant velocity and temperature gradients of the turbulent carrier gas flow in the jet cross sections increase the probability of appearance of non-melted particles in the zone of coating formation.

The loss of the particle mass due to evaporation, which exerts a significant effect on the particle dynamics, has to be minimized. Figure 8 illustrates the process of particle evaporation depending on the initial particle size. The evaporation process begins at $z = z_1$ and ends at $z = z_2$, when the entire mass of the particle becomes evaporated. An increase in the particle size leads to an increase in the coordinate of the point of particle evaporation. The relative particle mass loss due to evaporation is approximately 5%. A nonmonotonic behavior of the parameter z_2 as a function of the particle size should be noted.

Conclusions. A mathematical model of the flow in a turbulent nonisothermal jet with particles is constructed. The model takes into account the migration mechanism of particle motion under the action of turbulent fluctuations of the carrier flow velocity, as well as melting and evaporation of an individual particle.

The model constructed is valid in a wide range of parameters at the nozzle exit, because the method of integral relations is used to calculate the characteristics of the carrier gas in the case of intense heating of the jet.

Factors that restrict the area of applicability of the model are the assumption that the velocity fluctuations of the turbulent carrier flow obey the normal distribution law and the neglect of particle collisions. Particle collisions may be neglected if the volume concentration of particles is very low (about 10^{-6}). The assumption of the normal distribution of velocity fluctuations is approximate, which is taken into account by introducing damping functions constructed on the basis of experimental data on the microstructure of jet flows. To expand the areas of applicability of the model for calculating the fluctuating parameters of the carrier flow, one has to use turbulence models that take into account the nonisotropic character of turbulent viscosity.

The conditions of particle insertion into the jet flow (velocity of injection, streamwise or crossflow injection) have a substantial effect on the character of particle motion, heating, and scattering due to the migration mechanism of transport. The velocity of particle injection at the nozzle exit affects the particle coordinates corresponding to the beginning of particle melting and evaporation. The dependences of these coordinates on the particle radius are close to parabolas, and the dependences of velocities acquired by the particles at the points with these coordinates on the particle radius are close to straight lines. The relative loss of the particle mass due to evaporation reaches approximately 5%.

Mixing of the jet with the ambient quiescent fluid leads to a significant statistical scattering of particle velocities and temperatures (both local values and values over the jet cross section), which, in turn, is responsible for the higher inhomogeneity of the structure of the deposited coating, for the lower coating density, and for the worse strength of adhesion.

REFERENCES

1. C. T. Crowe, T. R. Troutt, and J. N. Chung, "Numerical models for two-phase turbulent flows," *Annu. Rev. Fluid Mech.*, **28**, 11–43 (1996).
2. K. N. Volkov, "Stochastic modeling of particle motion and scattering in mechanics of turbulent gas-disperse flows," *Inzh.-Fiz. Zh.*, **77**, No. 5, 10–20 (2004).
3. K. N. Volkov and G. F. Gorshkov, "Stochastic modeling of scattering of the disperse phase in turbulent jets," *Mat. Model.*, **14**, No. 10, 77–82 (2002).
4. K. N. Volkov and G. F. Gorshkov, "Scattering and heat transfer of disperse-phase particles in turbulent non-isothermal jets of a gas and low-temperature plasma," *Inzh.-Fiz. Zh.*, **77**, No. 2, 51–57 (2004).
5. S. I. Navoznov, A. A. Pavel'ev, A. S. Mul'gi, and M. K. Laats, "Effect of initial slipping on particle scattering in a two-phase jet," in: *Turbulent Two-Phase Flows* (collected scientific papers) [in Russian], Izd. Tallin. Politekh. Inst., Tallin (1979), pp. 149–157.
6. T. A. Girshovich, A. I. Kartushinskii, and M. K. Laats, "Experimental study of a turbulent jet carrying heavy admixtures," *Izv. Akad. Nauk SSSR, Mekh. Zhidk. Gaza*, No. 5, 26–31 (1981).
7. H.-B. Xiong, L.-L. Zheng, S. Sampath, et al., "Three-dimensional simulation of plasma spray: effects of carrier gas flow and particle injection on plasma jet and entrained particle behavior," *Int. J. Heat Mass Transfer*, **47**, No. 24, 5189–5200 (2004).
8. D. T. Gawne, B. Liu, Y. Bao, and T. Zhang, "Modelling of plasma-particle two-phase flow using statistical techniques," *Surface Coat. Technol.*, **191**, Nos. 2/3, 242–254 (2005).
9. G. Mariaux and A. Vardelle, "3-D time-dependent modelling of the plasma spray process. Flow modelling," *Int. J. Thermal Sci.*, **44**, No. 4, 357–366 (2005).
10. F. Qunbo, W. Lu, and W. Fuchi, "3D simulation of the plasma jet in thermal plasma spraying," *J. Mater. Proc. Technol.*, **166**, No. 2, 224–229 (2005).
11. K. Ramachandran and V. Selvarajan, "Trajectory and temperature history of the particles of different sizes and their injection velocities in a thermal plasma," *Comput. Mater. Sci.*, **6**, No. 1, 81–91 (1996).
12. V. V. Sobolev, J. M. Guilemany, and A. J. Martin, "In-flight behaviour of steel particles during plasma spraying," *J. Mater. Proc. Technol.*, **87**, Nos. 1/3, 37–45 (1999).
13. W. A. Sirignano, *Fluid Dynamics and Transport of Droplets and Sprays*, Cambridge Univ. Press, Cambridge (1999).
14. L. A. Dombrovsky and S. S. Sazhin, "A parabolic temperature profile model for heating of droplets," *Trans. ASME, J. Heat Transfer*, **125**, 535–537 (2003).

15. L. A. Dombrovsky and S. S. Sazhin, "A simplified non-isothermal model for droplet heating and evaporation," *Int. Communic. Heat Mass Transfer*, **30**, 787–796 (2003).
16. G. F. Gorshkov, "Propagation of variable-composition cocurrent nonisothermal jets of a gas and plasma," in: *Dynamics of Inhomogeneous and Compressible Media* (collected scientific papers) [in Russian], Izd. Leningr. Gos. Univ., Leningrad (1984), pp. 164–175.
17. L. E. Sternin and A. A. Shraiber, *Multiphase Gas–Particle Flows* [in Russian], Mashinostroenie, Moscow (1994).
18. K. N. Volkov, "Difference schemes of integration of equations of motion of a test particle in a liquid or gas flow," *Vychisl. Metody Programm.*, **5**, No. 1, 5–21 (2004).
19. N. B. Vargaftik, *Thermophysical Properties of Substances: Handbook* [in Russian], Mashinostroenie, Moscow (1972).